

Measurement of $dE_T/d\eta$ in Au+Au Collisions at 200 GeV with the sPHENIX detector

The sPHENIX Collaboration

Abstract

The transverse energy in heavy ion collisions is one of the key observables characterizing global properties of the quark-gluon plasma (QGP). The transverse energy per unit pseudorapidity ($dE_T/d\eta$) probes the energy carried by the medium along the longitudinal direction, providing essential information related to the initial geometry propagated through subsequent hydrodynamic evolution of the QGP. This note reports preliminary measurements of $dE_T/d\eta$ from the sPHENIX experiment using the Relativistic Heavy Ion Collider's (RHIC) 2023 Commissioning dataset of Au+Au collisions at 200 GeV. These results are the first $dE_T/d\eta$ measurements at RHIC energies from a hadronic calorimeter with full azimuthal coverage. Results are compared to previous measurements of $dE_T/d\eta$ for 200 GeV Au+Au collisions at RHIC made with only electromagnetic calorimetry.

1 Introduction

Fundamental aspects of the nuclear strong force can be studied in heavy ion collisions, which produce hot and dense matter consisting of deconfined quarks and gluons, known as the quark-gluon plasma (QGP) [1]. The characteristics of the QGP can be assessed by measuring the properties of the final state particles produced after the full evolution of the medium [2]. An important quantity to study such properties is the transverse energy per unit pseudorapidity, $dE_T/d\eta$, which measures the energy carried by the medium along the longitudinal direction, providing essential information related to the initial geometry propagated through subsequent hydrodynamic evolution of the QGP [3].

Previous $dE_T/d\eta$ measurements from the PHENIX [4] and STAR [5] collaborations at RHIC have measured Bjorken energy densities in Au+Au collisions at nucleon-nucleon center-of-mass energy of $\sqrt{s_{NN}} = 200$ GeV greater than $4 \text{ GeV}/\text{fm}^3$ [5, 6, 7]. These measurements have successfully demonstrated a necessary condition of QGP production for such collisions by measuring energy densities above Lattice QCD predictions for the transition to QGP [8]. Similar characteristics have been noted in various experiments at the LHC with Pb+Pb collisions at higher energies [9, 10]. The centrality dependence of $dE_T/d\eta$, and its interpretation in terms of geometric quantities such as average number of nucleon participants ($\langle N_{\text{part}} \rangle$) has also been investigated in these experiments.

The sPHENIX detector is a new detector located at RHIC, designed to provide qualitatively new capabilities. In particular, the calorimetry system is composed of the Electromagnetic Calorimeter (EMCal) and the first Hadronic Calorimeter (HCal) with full azimuthal coverage employed at RHIC energies. Purpose built for high-precision measurements of jets, hadrons, and photons, the sPHENIX calorimetry system is well-suited for a precision measurement of $dE_T/d\eta$. Furthermore, the detailed study of the energy deposits of the sPHENIX calorimeters is essential for the development of the sPHENIX jet physics program [11, 12].

This note reports a measurement of $dE_T/d\eta$ in Au+Au collisions at $\sqrt{s_{NN}} = 200$ GeV with the sPHENIX detector using the Run 2023 commissioning dataset. It is the first measurement employing a hadronic calorimeter at RHIC energies. The results are presented as functions of pseudorapidity (η) in different Au+Au collision centrality intervals.

2 sPHENIX detector

The sPHENIX detector is located at RHIC and employs both tracking and calorimeter subsystems in order to make measurements of the heavy ion and proton-proton collisions provided by RHIC beams. sPHENIX has three calorimeter layers, an Electromagnetic Calorimeter (EMCal) and an Inner Hadronic Calorimeter (IHCal) and an Outer Hadronic Calorimeter (OHCal) separated by a 1.4T superconducting magnet which was on for this Run 2023 dataset. These detectors are concentric, with the EMCal located closest to the interaction point and the OHCal located furthest from the interaction point within the calorimeter system. These detectors have full azimuthal coverage and coverage of $|\eta| < 1.1$ in pseudorapidity.

The sPHENIX EMCal [13, 14] is 20.1 radiation lengths deep and is designed to measure photons, electrons and positrons via electromagnetic showers. The sPHENIX EMCal is a sam-

pling calorimeter made of a tungsten powder absorber and scintillating fibers with tower size $\Delta\eta \times \Delta\phi = 0.024 \times 0.024$. The light from the scintillating fibers is collected by a light guide and processed into voltage signals using silicon photomultipliers (SiPMs). The EMCal also measures 0.83 hadronic interaction lengths and therefore sees a significant amount of hadronic shower energy.

The sPHENIX HCal system is designed to measure hadronic showers with the full EMCal + HCal system totaling 4.9 hadronic interaction lengths. Both the IHCal and OHCal are sampling calorimeters comprising aluminum (inner)/steel (outer) absorbing plates and scintillating tiles with tower size $\Delta\eta \times \Delta\phi = 0.1 \times 0.1$. Both IHCal and OHCal scintillating tiles are set at an angle offset to the transverse direction to reduce the amount of traversing particles that do not interact with the active volumes of these calorimeters. The light from these tiles is then also processed by SiPMs [14].

This analysis uses data from all three calorimeters as well as global event information, such as the collision vertex and the centrality of the event, from the Minimum Bias Detector (MBD). The MBD is located at forward rapidity, $3.51 < |\eta| < 4.61$, on both sides of the interaction point interaction point, close to the beam pipe, and comprises 128 channels of photomultiplier tubes (PMTs). The MBD is used for triggering on *minimum-bias* (MB) events in heavy ion collisions and for collision vertex determination. The MBD was previously used in PHENIX at $3.0 < |\eta| < 3.9$ [15] where it was also used for triggering on MB events and z-vertex and centrality determination.

The sPHENIX Zero Degree Calorimeter (ZDC) [16] is located on both sides of the interaction point (IP), at a distance of 18 m from the IP. It is a sampling hadronic calorimeter comprised of tungsten alloy and PMMA-based optical fiber. These fibers transmit Cherenkov light generated from secondaries charged particles of hadronic showers to PMTs. The ZDC is incorporated into the MB criteria to differentiate MBD triggered events from beam background.

3 Analysis

3.1 Event selection

Events are selected using a hardware trigger requiring at least two photomultiplier tubes fired on both sides of the MBD. In the offline analysis, a set of MB selection criteria using the MBD and the ZDC was applied based on the expected correlations between signals in different detectors to remove beam-related backgrounds and non-hadronic collisions. In addition, a z-vertex cut, $|z_{vtx,MBD}| < 20$ cm, has been applied to avoid peripheral events in the tail of the distribution with large vertex resolution. The z-vertex was determined using the timing channels of the MBD.

Centrality percentiles were derived by fitting the MBD charge distribution through a convolution of particle production and event sampling based on a negative binomial distribution from Monte Carlo (MC) Glauber simulation [17, 18, 19]. Events are selected in the centrality range of 0–60% to ensure high event selection efficiency with a broad range of geometric configuration of the medium. The event selection achieved complete efficiency under the specified selection criteria.

In this analysis, we used eight runs recorded in July 2023 as part of the commissioning process of the sPHENIX detector in Run-2023, during which the MBD and calorimeters were in a normal

operational mode. Applying all the specified cuts, this dataset yields 249k events.

Three different MC event generators HIJING [20], AMPT [21] and EPOS [22] were used for this analysis to derive correction factors to extract $dE_T/d\eta$ from the sPHENIX calorimeter measurements, with HIJING being used to derive the nominal results. The MC events were weighted to match the z -vertex distribution in data. To account for any discrepancies in the particle spectra between MC simulation and data, the generator-level spectra are weighted to the measured identified particle spectra previously measured by PHENIX [23] and STAR [24]. The transverse momentum (p_T) spectra were analyzed for each particle species across various centrality intervals and then compared to that in MC simulation. The particles in the MC samples are then reweighted using data over MC ratios determined for each particle species, p_T , and event centrality.

3.2 $dE_T/d\eta$ measurement

The time-sampled electronic signals from each calorimeter tower are processed using a template fit created from Run 2023 data and calibrated to the electromagnetic energy scale, meaning that they report, on average, the correct energy deposited by EM particles. For the EMCal, the absolute energy scale calibration is established from an η -dependent calibration of the π^0 meson peak in data to the same position as in simulation, using the runs within this measurement's dataset. The η region for the EMCal is limited to $-0.9 < \eta < 1.1$ because the EMCal readout electronics were only partially instrumented during this stage of commissioning. The IHCAL and OHCAL absolute EM energy scale calibration is performed using the minimum ionizing particle energy depositions from cosmic ray muons from data taken in early 2024. Temperature-dependent corrections to the detector energy scale are applied to these cosmic calibrations to account for gain variations from detector conditions during collision data-taking. Low energy noise waveforms are processed using a peak-minus-pedestal offline zero suppression algorithm at an ADC threshold which corresponds to negligible contributions to $dE_T/d\eta$ from noise; optimal thresholds of 60/15/90 MeV for the sPHENIX EMCal/IHCAL/OHCAL towers were found using pedestal data to ensure that calorimeter noise is fully suppressed and has negligible contributions to $dE_T/d\eta$.

The uncorrected $dE_T/d\eta$ is calculated for a given centrality class as the sum of calorimeter tower E_T as a function of η , where E_T for each calorimeter tower is

$$E_{T,tower} = E_{tower} \sin(\theta_{tower}) \quad (1)$$

The simulations described above were used to correct the reconstructed energy for the response of the calorimeters. Events from each of these MC generators are passed through a GEANT4 [25] simulation of the sPHENIX detector as part of determining the correction factor from uncorrected $dE_T/d\eta$ to truth $dE_T/d\eta$.

The generator-level $dE_T/d\eta$ is calculated from the particle information of the reweighted HIJING dataset by summing the $E_{T,particle}$ for all final state particles within the detector's acceptance as a function of η . The reconstructed $dE_T/d\eta$ in simulation is found in the same manner as the uncorrected $dE_T/d\eta$ from calorimeter towers in data. Correction factors are created for each calorimeter sub-system and each centrality bin using the mean reconstructed transverse energy distribution in the specific calorimeter divided by the truth transverse energy distribution for that centrality class.

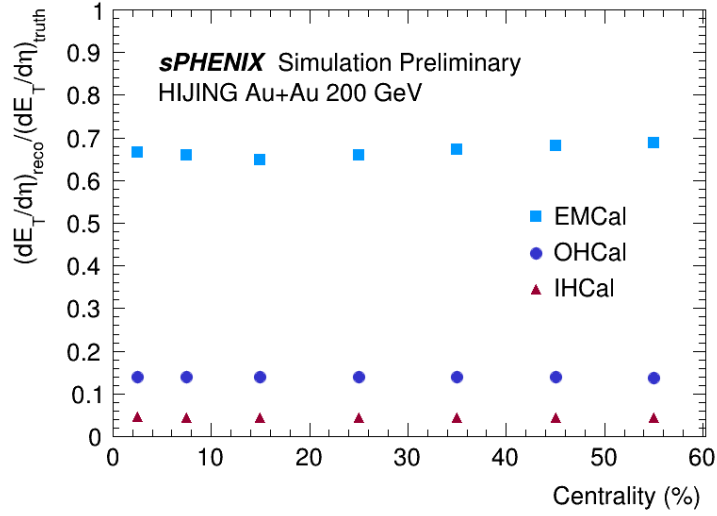


Figure 1: Mean correction factor value of reconstructed $dE_T/d\eta$ for $|\eta| < 0.5$ divided by generator level $dE_T/d\eta$ for sPHENIX calorimeter sub-systems as a function of centrality for range 0-60% centrality.

$$C(\eta) = \frac{\sum E_{T,tower}(\eta)}{\sum E_{T,particle}(\eta)} \quad (2)$$

The derived correction factors also take into account areas of the calorimeters which were inactive during the commissioning data-taking period to be consistent with the detector acceptance in data.

The correction factors for each calorimeter sub-system are fairly constant with centrality, with about 66% of total $dE_T/d\eta$ reconstructed by the EMCAL, about 14% reconstructed by the OHCAL and about 4% of the E_T reconstructed by the IHCAL in the calorimeter η acceptance with both the IHCAL and OHCAL calibrated to the EM scale. The ratio of reconstructed $dE_T/d\eta$ to truth $dE_T/d\eta$ for each calorimeter layer as a function of centrality can be found in Fig. 1.

In this analysis, the EMCAL and full HCal (IHCAL + OHCAL) are used to make standalone measurements of the $dE_T/d\eta$ and all three calorimeter layers (EMCAL + IHCAL + OHCAL) are used for a full calorimeter measurement of $dE_T/d\eta$, where:

$$\frac{dE_T}{d\eta}(\eta) = \frac{\sum E_{T,tower}(\eta)}{C(\eta)} \quad (3)$$

3.3 Systematic uncertainties

The uncertainty contributions to the measurement include the calorimeter energy response, the application of the particle spectra reweighing in simulation, calorimeter noise processing, detector acceptance, and z-vertex resolution effects.

	Calibration	Hadronic response	MC	ZS	Accept.	Z-vertex	Total
EMCal	1.5-1.7	3.0	1.0-1.2	0.3-2.0	0.5-0.9	0.2	3.7-4.3
OHCAL	1.2-1.3	3.4-3.6	2.9-4.3	0.3-0.4	0.7-1.2	0.4	5.1-6.0
Full Calo	1.2-1.3	3.0-3.1	1.4-1.9	0.2-1.6	0.4-0.9	0.2	3.8-4.2

Table 1: Summary of mean systematic uncertainties over measurement η range for $dE_T/d\eta$ measurements from each calorimeter for the full range of measurement centrality bins. Uncertainty values listed above are given in percentages. Listed hadronic response uncertainty only includes MC contributions presently. MC uncertainty refers to the uncertainty related to correction factors derived from MC.

The calorimeter energy response includes the uncertainties in the absolute energy calibration and hadronic response modeling. The total effect of calorimeter EM-scale calibration systematics is 1.2%-1.7% for all calorimeter sub-systems over all centrality bins studied in this measurement. To estimate our sensitivity to the hadronic response modeling, two variations of GEANT configuration lists, FTFP.BERT_HP and QGSP.BERT_HP, are compared to the nominal configuration using FTFP.BERT; this results in a variation across the full η measurement range of at most 3% in the EMCal, 2% in the IHCAL and 4% in the OHCAL. Additional uncertainties regarding differences of the calorimeter's hadronic and electromagnetic response and subsystem energy resolution effects are not evaluated in the present analysis.

To estimate the uncertainty associated with the correction for the detector response, we find the variation in applying our reweighting scheme to three different generators, HIJING, AMPT and EPOS. Furthermore, the nominal reweighting based on PHENIX and STAR spectra at central η is compared to an additional method of particle spectra reweighting which is differential in transverse momentum and rapidity using data from BRAHMS [26, 27].

Additional sub-dominant uncertainties associated with a number of other potential effects are described below. We vary the ADC threshold at which we switch from waveform processing using zero suppression to using the template fit by ± 10 ADC to estimate the uncertainty in processing noise; this variation results in a $< 1\%$ difference in central collisions and about 2.0% in peripheral events. Additionally, the reconstructed z-vertex is shifted by 3 cm as a conservative estimate of the uncertainty in z-vertex reconstruction from the MBD; this results in a $< 1\%$ deviation for all measurements. Finally, to determine the effect of the changing calorimeter acceptance run by run, we find the variation in $dE_T/d\eta$ on a run by run basis. The standard deviation of this run group is between 0.5% and 1% for all $dE_T/d\eta$ measurements in all centrality bins which is within the statistical uncertainty in the $dE_T/d\eta$ measurements.

The total uncertainties for $dE_T/d\eta$ are determined as a function of η for each calorimeter measurement and each centrality bin. The total systematic uncertainty as well as contributing uncertainties at $\eta = 0$ are shown in Table 1 for all centrality bins. The mean total uncertainty on $dE_T/d\eta$ for EMCal and full calorimeter measurements over the full η measurement range is generally around 4%. The largest uncertainty contribution coming from the uncertainty in hadronic response for EMCal-only results. The total uncertainty on $dE_T/d\eta$ from the full calorimeter has largest uncertainty contributions from the MC hadronic response modeling and the MC reweighting. For OHCAL-only results, the total uncertainty is between 5-6%; in central events the hadronic response uncertainty dominates and in peripheral events the MC reweighting is the largest contribution.

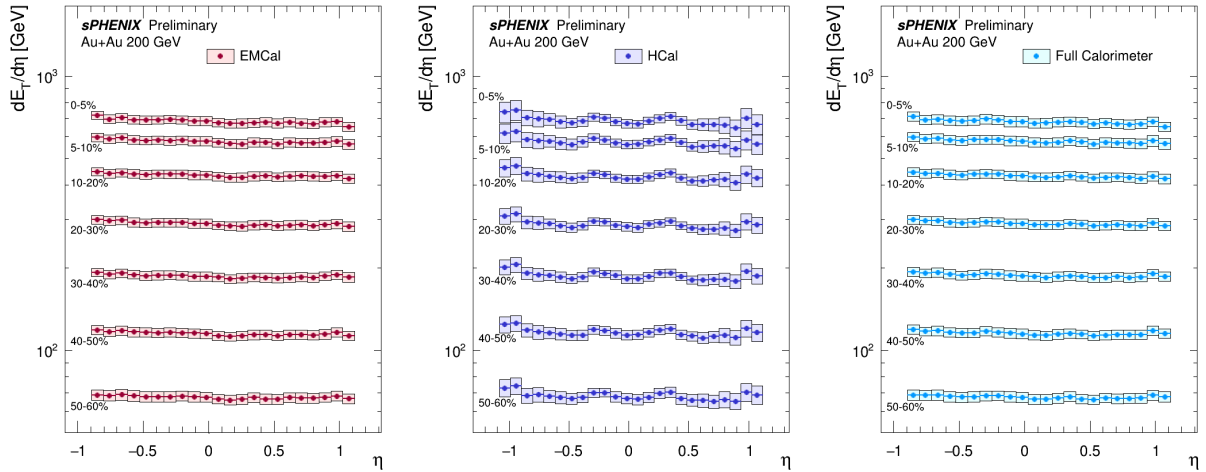


Figure 2: Fully corrected $dE_T/d\eta$ measurements over measurement range $-1.1 < \eta < 1.1$ for HCal-only results and $-0.9 < \eta < 1.1$ for EMCal-only and full calorimeter system results.

4 Results

Results for $dE_T/d\eta$ as a function of η are presented in Fig. 2 for various centrality intervals. The $dE_T/d\eta$ values for all three measurements with the sPHENIX EMCal, HCal and full calorimeter have a strong dependence on centrality, increasing towards more central Au+Au collisions, whereas no significant dependence on η is seen. Additionally, these measurements are consistent with one another within uncertainties.

In Fig. 3, the EMCal-only and HCal-only $dE_T/d\eta$ measurements are overlaid to highlight their agreement. This is a particularly encouraging result as the EMCal and HCal see different contributions of the collision energy. Further, for all calorimeter measurements, $dE_T/d\eta$ at positive η and negative η are compatible within uncertainties. Fig. 4 is included here to highlight the symmetric nature of the EMCal-only, HCal-only and full calorimeter $dE_T/d\eta$ results as a function of η .

Results from the sPHENIX full detector system for various centrality intervals are compared to the results from PHENIX [4] and STAR [5] in Fig. 5. The sPHENIX results are consistently higher than the results from PHENIX for all centrality bins but agree within uncertainties for mid-central bins 30-60%; the sPHENIX results are above the STAR results in the centrality range of 0-10% but are in agreement in other centrality intervals. Presently, these sPHENIX results use a preliminary centrality calculation for Run 2023 data which is likely to be updated for future reports of this analysis; therefore, conclusions on comparisons between sPHENIX and previous measurements are not presently made.

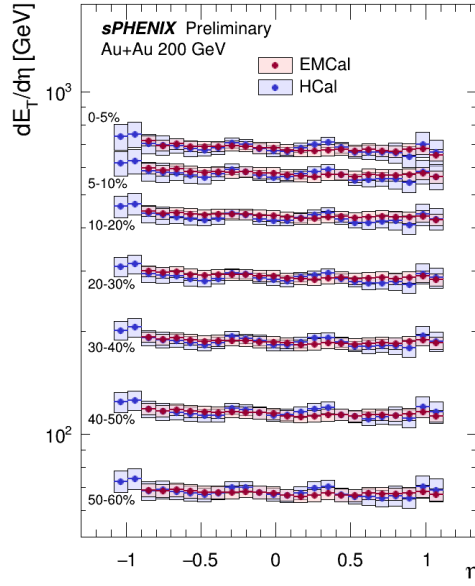


Figure 3: Comparison of fully corrected $dE_T/d\eta$ measurements for EMCal-only results ($-0.9 < \eta < 1.1$) and HCal-only results ($-1.1 < \eta < 1.1$).

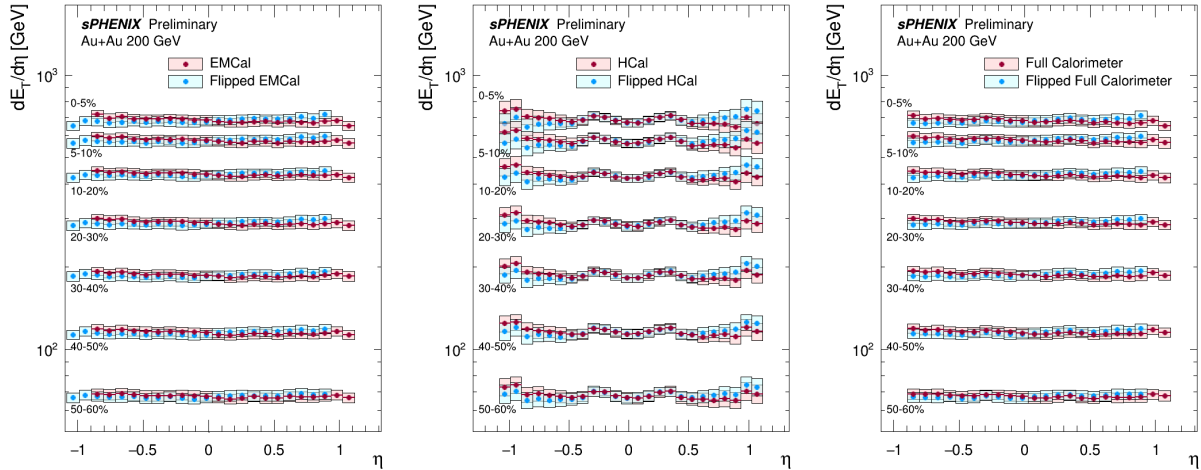


Figure 4: Comparison of fully corrected $dE_T/d\eta$ measurements over measurement range $-1.1 < \eta < 1.1$ for HCal-only results and $-0.9 < \eta < 1.1$ for EMCal-only and full calorimeter system results.

5 Summary

This note details a measurement of transverse energy per unit pseudorapidity ($dE_T/d\eta$) using commissioning data from Run 2023 in Au+Au collisions at $\sqrt{s_{NN}} = 200$ GeV collected with the sPHENIX detector. The $dE_T/d\eta$ is measured with the calorimeter system, including the hadronic calorimeter, which is used for the first time for such observables at RHIC.

Results are shown as a function of η using the EMCal-only, HCal-only and full calorimeter

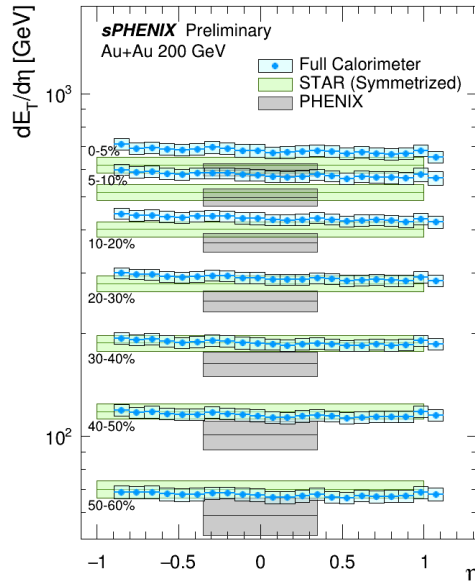


Figure 5: Fully corrected $dE_T/d\eta$ measurements over measurement range $-0.9 < \eta < 1.1$ using the full sPHENIX calorimeter system. STAR and PHENIX measurements are included for comparison.

system and full calorimeter results are compared to previous PHENIX and STAR results. These measurements are presented across a large centrality range showing a strong understanding of the sPHENIX calorimeter response over at least an order-of-magnitude in dynamic range and making this analysis a useful exercise towards accomplishing the sPHENIX jet physics program.

References

- [1] W. Busza, K. Rajagopal, and W. van der Schee. Heavy Ion Collisions: The Big Picture and the Big Questions. *Annual Review of Nuclear and Particle Science*, 68:339, 2018. doi:10.1146/annurev-nucl-101917-020852. 1
- [2] P. Romatschke and U. Romatschke. Relativistic fluid dynamics in and out of equilibrium – ten years of progress in theory and numerical simulations of nuclear collisions. 2017. arXiv:1712.05815. 1
- [3] S. Tiwari and R. Sahoo. Transverse Energy per Charged Particle in Heavy-Ion Collisions: Role of Collective Flow. *Eur. Phys. J. A*, 54:39, 2018. doi:10.1140/epja/i2018-12475-8. 1
- [4] A. Adare et al. (PHENIX Collaboration). Transverse energy production and charged-particle multiplicity at midrapidity in various systems from $\sqrt{s_{NN}} = 7.7$ to 200 GeV. *Phys. Rev. C*, 93:024901, 2016. doi:10.1103/PhysRevC.93.024901. 1, 4
- [5] J. Adams et al. (STAR Collaboration). Measurements of transverse energy distributions in Au + Au collisions at $\sqrt{s_{NN}} = 200$ GeV. *Phys. Rev. C*, 70:054907, 2004. doi:10.1103/PhysRevC.70.054907. 1, 4
- [6] J.T. Mitchell. Transverse Energy Measurements from the Beam Energy Scan in PHENIX. *Nuclear Physics A*, 956:842–845, 2016. The XXV International Conference on Ultrarelativistic

- Nucleus-Nucleus Collisions: Quark Matter 2015. doi:10.1016/j.nuclphysa.2016.01.041. 1
- [7] J. D. Bjorken. Highly relativistic nucleus-nucleus collisions: The central rapidity region. *Phys. Rev. D*, 27:140, 1983. doi:10.1103/PhysRevD.27.140. 1
- [8] F. Karsch. Lattice results on QCD thermodynamics. *Nuclear Physics A*, 698(1–4):199–208, February 2002. doi:10.1016/S0375-9474(01)01365-3. 1
- [9] J. Adams et al. (ALICE Collaboration). Measurement of transverse energy at midrapidity in Pb-Pb collisions at $\sqrt{s_{NN}} = 2.76$ TeV. *Physical Review C*, 94, 2016. doi:10.1103/physrevc.94.034903. 1
- [10] S. Chatrchyan et al. (CMS Collaboration). Measurement of the Pseudorapidity and Centrality Dependence of the Transverse Energy Density in Pb-Pb Collisions at $\sqrt{s_{NN}} = 2.76$ TeV. *Phys. Rev. Lett.*, 109:152303, 2012. doi:10.1103/PhysRevLett.109.152303. 1
- [11] A. Adare et al. An Upgrade Proposal from the PHENIX Collaboration, 2015. arXiv:1501.06197. 1
- [12] R. Belmont et al. Predictions for the sPHENIX physics program. *Nucl. Phys. A*, 1043:122821, 2024. doi:10.1016/j.nuclphysa.2024.122821. 1
- [13] C. A. Aidala et al. Design and Beam Test Results for the 2-D Projective sPHENIX Electromagnetic Calorimeter Prototype. *IEEE Transactions on Nuclear Science*, 68(2):173–181, 2021. doi:10.1109/TNS.2020.3034643. 2
- [14] C. A. Aidala et al. Design and Beam Test Results for the sPHENIX Electromagnetic and Hadronic Calorimeter Prototypes, 2018. arXiv:1704.01461. 2
- [15] M. Allen et al. PHENIX inner detectors. *Nuclear Instruments and Methods in Physics Research Section A: Accelerators, Spectrometers, Detectors and Associated Equipment*, 499(2):549–559, 2003. The Relativistic Heavy Ion Collider Project: RHIC and its Detectors. doi:10.1016/S0168-9002(02)01956-3. 2
- [16] C Adler, A Denisov, E Garcia, M Murray, H Stroebele, and S White. The RHIC zero degree calorimeters. *Nuclear Instruments and Methods in Physics Research Section A: Accelerators, Spectrometers, Detectors and Associated Equipment*, 470(3):488–499, 2001. doi:10.1016/S0168-9002(01)00627-1. 2
- [17] C. Loizides, J. Nagle, and P. Steinberg. Improved version of the PHOBOS Glauber Monte Carlo. *SoftwareX*, 1–2:13–18, September 2015. doi:10.1016/j.softx.2015.05.001. 3.1
- [18] S. S. Adler et al. (PHENIX Collaboration). Systematic studies of the centrality and $\sqrt{s_{NN}}$ dependence of the $dE_T/d\eta$ and $dN_{ch}/d\eta$ in heavy ion collisions at midrapidity. *Phys. Rev. C*, 71:034908, Mar 2005. doi:10.1103/PhysRevC.71.034908. 3.1
- [19] A. Adare et al. (PHENIX Collaboration). Centrality categorization for $R_{p(d)+A}$ in high-energy collisions. *Phys. Rev. C*, 90:034902, Sep 2014. doi:10.1103/PhysRevC.90.034902. 3.1
- [20] X. Wang and M. Gyulassy. HIJING: A Monte Carlo model for multiple jet production in pp, pA, and AA collisions. *Phys. Rev. D*, 44:3501–3516, Dec 1991. doi:10.1103/PhysRevD.44.3501. 3.1
- [21] Z. Lin, C. Ko, B. Li, B. Zhang, and S. Pal. Multiphase transport model for relativistic heavy ion collisions. *Physical Review C*, 72(6), December 2005. doi:10.1103/physrevc.72.064901. 3.1

- [22] T. Pierog, Iu. Karpenko, J. M. Katzy, E. Yatsenko, and K. Werner. EPOS LHC: Test of collective hadronization with data measured at the CERN Large Hadron Collider. *Physical Review C*, 92(3), September 2015. doi:10.1103/physrevc.92.034906. 3.1
- [23] A. Adare et al. (PHENIX Collaboration). Spectra and ratios of identified particles in Au+Au and d +Au collisions at $\sqrt{s_{NN}} = 200$ GeV. *Phys. Rev. C*, 88:024906, Aug 2013. doi:10.1103/PhysRevC.88.024906. 3.1
- [24] J. Adams et al. (STAR Collaboration). Scaling Properties of Hyperon Production in Au + Au Collisions at $\sqrt{s_{NN}} = 200$ GeV. *Phys. Rev. Lett.*, 98:062301, Feb 2007. doi:10.1103/PhysRevLett.98.062301. 3.1
- [25] S. Agostinelli et al. GEANT4—a simulation toolkit. *Nucl. Instrum. Meth. A*, 506:250–303, 2003. doi:10.1016/S0168-9002(03)01368-8. 3.2
- [26] I. G. Bearden et al. (BRAHMS Collaboration). Nuclear Stopping in Au + Au Collisions at $\sqrt{s_{NN}} = 200$ GeV. *Phys. Rev. Lett.*, 93:102301, Aug 2004. doi:10.1103/PhysRevLett.93.102301. 3.3
- [27] I. G. Bearden et al. (BRAHMS Collaboration). Charged Meson Rapidity Distributions in Central Au + Au Collisions at $\sqrt{s_{NN}} = 200$ GeV. *Phys. Rev. Lett.*, 94:162301, Apr 2005. doi:10.1103/PhysRevLett.94.162301. 3.3